J Neurophysiol
87: 2612–2623, 2002; 10.1152/jn.00667.2001.

Role for G Protein G$\beta\gamma$ Isoform Specificity in Synaptic Signal Processing: A Computational Study

RICHARD BERTRAM,[1] MICHELLE I. ARNOT,[2] AND GERALD W. ZAMPONI[2]
[1]*Department of Mathematics and Kasha Laboratory of Biophysics, Florida State University, Tallahassee, Florida 32306; and* [2]*Department of Physiology and Biophysics, University of Calgary, Calgary, Alberta T2N 4N1, Canada*

Received 9 August 2001; accepted in final form 28 December 2001

Bertram, Richard, Michelle I. Arnot, and Gerald W. Zamponi. Role for G protein G$\beta\gamma$ isoform specificity in synaptic signal processing: A computational study. *J Neurophysiol* 87: 2612–2623, 2002; 10.1152/jn.00667.2001. Computational modeling is used to investigate the functional impact of G protein–mediated presynaptic autoinhibition on synaptic filtering properties. It is demonstrated that this form of autoinhibition, which is relieved by depolarization, acts as a high-pass filter. This contrasts with vesicle depletion, which acts as a low-pass filter. Model parameters are adjusted to reproduce kinetic slowing data from different G$\beta\gamma$ dimeric isoforms, which produce different degrees of slowing. With these sets of parameter values, we demonstrate that the range of frequencies filtered out by the autoinhibition varies greatly depending on the G$\beta\gamma$ isoform activated by the autoreceptors. It is shown that G protein autoinhibition can enhance the spatial contrast between a spatially distributed high-frequency signal and surrounding low-frequency noise, providing an alternate mechanism to lateral inhibition. It is also shown that autoinhibition can increase the fidelity of coincidence detection by increasing the signal-to-noise ratio in the postsynaptic cell. The filter cut, the input frequency below which signals are filtered, depends on several biophysical parameters in addition to those related to G$\beta\gamma$ binding and unbinding. By varying one such parameter, the rate at which transmitter unbinds from autoreceptors, we show that the filter cut can be adjusted up or down for several of the G$\beta\gamma$ isoforms. This allows for great synapse-to-synapse variability in the distinction between signal and noise.

INTRODUCTION

The importance of Ca^{2+} flux through voltage-dependent ion channels cannot be overstated. Calcium entering the cell through this pathway participates in muscle contraction, gene expression, synaptic transmission, and various forms of short- and long-term memory (Bito et al. 1997; Tsien and Tsien 1990). It is therefore not surprising that Ca^{2+} channels are subject to control through a myriad of electrical, biochemical, and genetic pathways. In recent years there have been numerous studies on Ca^{2+} channel regulation through G protein signaling (for example, Arnot et al. 2000; Bean 1989; Boland and Bean 1993; Chen and van den Pol 1998; Dittman and Regehr 1996; Garcia et al. 1998; Patil et al. 1996; Ruiz-Velasco and Ikeda 2000; Stanley and Mirotznik 1997; Zamponi and Snutch 1998). Channel regulation may be due to the direct action of activated G proteins or may involve additional second-messenger pathways (Diversé-Pierluissi et al. 2000). The focus of the present study is on functional implications of direct regulation of N-type Ca^{2+} channels, where it has been established that the G$\beta\gamma$ subunits of activated G proteins bind directly to the channels at the cytoplasmic linker region between domains I and II of the α_1 subunit and also at the carboxyl terminal region (Herlitze et al. 1996; Ikeda 1996; Zamponi et al. 1997; Zhang et al. 1996). Such binding puts channels into a reluctant state, reducing the net Ca^{2+} flux into the cell (Bean 1989). This inhibition can be relieved by depolarization (Bean 1989), which results in unbinding of G$\beta\gamma$ from the channel (Zamponi and Snutch 1998).

Two defining characteristics of voltage-dependent G protein–mediated Ca^{2+} channel inhibition are "kinetic slowing" (Patil et al. 1996), whereby the Ca^{2+} current time course is slowed in the presence of G protein agonists, and "prepulse facilitation" (Boland and Bean 1993), whereby the Ca^{2+} current evoked by a voltage pulse is facilitated if preceded by a depolarizing prepulse. Recent studies have shown that the extent of kinetic slowing and prepulse facilitation depend greatly on the specific G protein β and γ subunits involved. This was shown for native N-type Ca^{2+} channels in the presence of transfected G$\beta\gamma$ dimers in cervical ganglion cells (Garcia et al. 1998; Ruiz-Velasco and Ikeda 2000) and for N-type (Zhou et al. 2000) or N- and P-type Ca^{2+} channels co-transfected with G$\beta\gamma$ dimers in human embryonic kidney cells (Arnot et al. 2000). G$\beta\gamma$ specificity raises the possibility that a single agonist, such as glutamate or norepinephrine, can bind to different receptor types and activate several G$\beta\gamma$ dimeric isoforms within the same cell or cell compartment, each dimer having a distinct inhibitory action on the Ca^{2+} channels.

Although inhibition of Ca^{2+} channels can have many functional ramifications in neurons, the focus of the present study is the role that G protein inhibition may play in signal processing at the synapse by regulating the probability of synaptic transmitter release. Exocytosis of synaptic transmitters occurs upon binding of Ca^{2+} to proteins associated with the vesicle fusion machinery. The source of this Ca^{2+} is influx through Ca^{2+} channels, primarily N- and P-type, colocalized with synaptic vesicles (Llinás et al. 1992; Simon and Llinás 1985). It has been demonstrated that bath application of G protein agonists reduce transmitter release by inhibiting Ca^{2+} channels (Boehm

Address for reprint requests: R. Bertram, Dept. of Mathematics, Florida State University, Tallahassee, FL 32306 (E-mail: bertram@math.fsu.edu).

The costs of publication of this article were defrayed in part by the payment of page charges. The article must therefore be hereby marked "*advertisement*" in accordance with 18 U.S.C. Section 1734 solely to indicate this fact.

and Betz 1997; Chen and van den Pol 1997; Dittman and Regehr 1996; Qian et al. 1997; Takahashi et al. 1998; Wu and Saggau 1994). Recently, $G\beta\gamma$ subunits were injected directly into the large calyx of Held synapse by whole cell patch pipettes, and shown to inhibit P-type Ca^{2+} channels (Kajikawa et al. 2001). Other studies have shown that facilitation of transmitter release was enhanced by G protein agonists (Brody and Yue 2000; Dittman and Regehr 1997; Dunwiddie and Haas 1985; Isaacson et al. 1993; Shen and Johnson 1997). These latter studies are consistent with data showing that trains of short action potential–like depolarizations can relieve G protein inhibition of N-type channels in central neurons (Williams et al. 1997) and recombinant P/Q-type Ca^{2+} channels in HEK cells (Brody et al. 1997). Taken together, these data provide strong evidence that G protein inhibition and voltage-dependent relief of inhibition may play an important role in short-term synaptic plasticity. This was explored in a computational study, where it was demonstrated that the facilitory effects of residual Ca^{2+} can be compounded by relief of channel inhibition, significantly augmenting short-term synaptic enhancement (Bertram and Behan 1999).

Activation of G proteins is achieved through the binding of hormones or neurotransmitters to G protein–coupled receptors, leading to dissociation of $G\alpha$ and $G\beta\gamma$ subunits. One intriguing pathway involves the release of neurotransmitters and subsequent binding onto the same presynaptic terminal. Autoinhibition of transmitter release then occurs as the result of the G protein–mediated inhibition of Ca^{2+} channels (Wu and Saggau 1997). In this report, we use computational modeling to address two questions: *1*) what is the role of G protein–mediated autoinhibition on synaptic signal processing, and *2*) how is signal processing affected by the different $G\beta\gamma$ isoforms? We employ a previously developed model for an N-type Ca^{2+} channel (Bertram and Behan 1999; Boland and Bean 1993) with G protein unbinding kinetics modified according to data for different $G\beta\gamma$ dimeric isoforms (Fig. 2) (Arnot et al. 2000). Although these data were obtained from HEK cells co-transfected with N-type channels ($\alpha_{1B} + \alpha_2 - \delta + \beta_{1b}$) and $G\beta\gamma$ dimers, the properties of the regulatory mechanism should be similar for similar channels and G proteins expressed in synapses.

Computational studies have shown previously that G protein autoinhibitory feedback on the presynaptic terminal acts like a high-pass filter, allowing high-frequency signals to pass through to the postsynaptic cell while attenuating and essentially filtering out low-frequency signals (Bertram 2001). Experimental support for this was provided by studies of bullfrog sympathetic ganglia, where presynaptic depression was prominent during 1- and 5-Hz stimulation, but not at 20 Hz (Shen and Horn 1996). This filtering is due to the kinetic slowing produced as activated $G\beta\gamma$ dimers accumulate. As we show here with 10-ms test pulses, kinetic slowing is expressed as a reduction in the initial slope of the Ca^{2+} current (Fig. 2), which would greatly reduce the amount of Ca^{2+} entering the terminal during an action potential. During high-frequency trains this inhibition is relieved as $G\beta\gamma$ dimers unbind from Ca^{2+} channels during the action potentials. Based on the present computational study, we predict that activation of different $G\beta\gamma$ isoforms leads to very different filtering properties. In particular, the range of frequencies over which signals are suppressed is different for different $G\beta\gamma$ isoforms.

We use network simulations to demonstrate that high-pass filtering removes low-frequency noise from input-layer (i.e., presynaptic) neurons, increasing the signal-to-noise ratio in the output layer (i.e., postsynaptic) neurons and enhancing the spatial contrast of the transmitted "image." Another mechanism for increasing spatial contrast has been described (Shepherd 1998), involving reciprocal inhibitory coupling of neighboring neurons. The novelty of the present mechanism is that no circuitry is required; all that is required is that input-layer neurons possess G protein–mediated autoinhibitory feedback.

We also consider signals produced by the concident firing of two or more high-frequency input cells. The fidelity of this type of signaling is degraded by low-frequency input, which can summate with a postsynaptic response from a high-frequency input to generate a "false positive" response. G protein–mediated autoinhibition reduces the input-layer noise, decreasing the number of false positive output-layer responses and so increasing the fidelity of coincidence detection.

Finally, we emphasize that the filtering characteristics associated with a specific $G\beta\gamma$ dimer depend on many biophysical parameters. We demonstrate this by varying the unbinding rate of a transmitter molecule from the presynaptic autoreceptor. Faster unbinding lowers the filter cut while slower unbinding raises the cut. These maneuvers effectively adjust the definitions of "signal" and "noise."

METHODS

Experimental

Human embryonic kidney-tsa201 cells (HEK-tsa201) were transiently transfected with cDNAs for N-type Ca^{2+} channels ($\alpha_{1B} + \alpha_2 - \delta + \beta_{1b}$), the $G\gamma_2$ subunit, and either the $G\beta_1$ or $G\beta_2$ subunit. cDNAs encoding calcium channels and G proteins, transient transfection of N-type Ca^{2+} channels, and patch-clamp recordings were the same as those previously described (Arnot et al. 2000). Briefly, currents were elicited by stepping from −100 mV to a test potential of +20 mV. Inhibition of Ca^{2+} channel current by G proteins was assessed by application of a strong depolarizing (+150 mV) prepulse (PP). The degree of inhibition caused by the G protein was determined as the ratio of absolute peak current amplitudes in the presence and absence of the PP (the *real facilitation*). These real facilitation ratios were obtained by varying the duration between the PP and the test pulse (Δt_1 = 2, 4, 6, 10, 15, 20, and 1,000 ms, Fig. 2*A*) and extrapolating to $\Delta t_1 = 0$. Peak amplitudes were normalized to current amplitude after a 1-s interpulse duration. Cells were compensated by 75–85%. Currents were analyzed using Clampfit (Axon Instruments) and fitted in Sigmaplot 4.0 (Jandel Scientific). A semiquantitative measure of activation time constants was established with monoexponential fits to the late rising phase of the raw current using Clampfit.

Presynaptic model

The presynaptic terminal is modeled as a single compartment, with equations for membrane potential, Ca^{2+}-dependent transmitter release, transmitter binding to autoreceptors, and Ca^{2+} influx through G protein–regulated channels (Fig. 1). The membrane potential (V) is described by a simplified form of the Hodgkin-Huxley equations (Hodgkin and Huxley 1952; Rinzel and Ermentrout 1989)

$$C_m \frac{dV}{dt} = -(I_{Na} + I_K + I_{leak} - I_{app}) \quad (1)$$

$$\frac{dn}{dt} = \alpha_n(1 - n) - \beta_n n \quad (2)$$

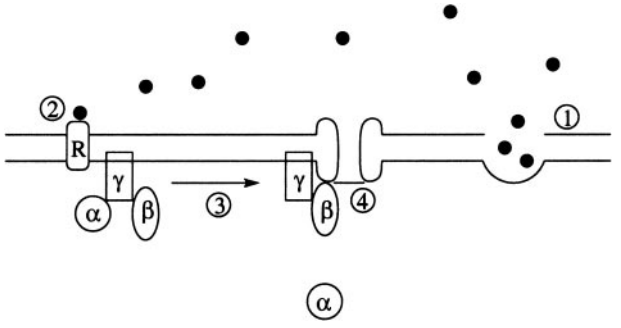

FIG. 1. Illustration of the presynaptic model. Vesicle fusion and transmitter release occur when a Ca^{2+} ion binds to a low-affinity binding site (1), binding of a transmitter molecule to a presynaptic autoreceptor activates a G protein (2), the G$\beta\gamma$ dimer binds to an N-type Ca^{2+} channel (3), the bound channel is put into a reluctant state (4).

where $C_m = 1\ \mu\text{Fcm}^{-2}$ is the membrane capacitance, $I_{\text{Na}} = 120x_\infty^3(1-n)(V-120)$, $I_{\text{K}} = 36n^4(V+77)$, $I_{\text{leak}} = 0.3(V+54)$ (μAcm^{-2}) are endogenous currents, I_{app} is an external current applied periodically (40 μAcm^{-2}) to evoke action potentials, and n is an activation variable for the K^+ current, with $\alpha_n = 0.02(V+55)/[1-e^{-(V+55)/10}]$ and $\beta_n = 0.25e^{-(V+65)/80}$. Since Ca^{2+} current often has little effect on the action potential in synapses (Sabatini and Regehr 1997; Takahashi et al. 1998), we omit this current from the voltage equation.

Flux of Ca^{2+} into the presynaptic terminal is through N-type Ca^{2+} channels. The model used here is based on a model of N-type G protein–regulated channels developed by Boland and Bean (1993), and simplified by Bertram and Behan (1999). This has three G protein bound "reluctant" closed states (C_{G1}–C_{G3}), four "willing" closed states (C_1–C_4), and one willing open state (O)

$$\begin{array}{ccccccc} C_1 & \underset{\beta}{\overset{4\alpha}{\rightleftarrows}} & C_2 & \underset{2\beta}{\overset{3\alpha}{\rightleftarrows}} & C_3 & \underset{3\beta}{\overset{2\alpha}{\rightleftarrows}} & C_4 \underset{4\beta}{\overset{\alpha}{\rightleftarrows}} O \\ k_G^- \downarrow k_G^+ & & k_{G2}^- \downarrow k_G^+ & & k_{G3}^- \downarrow k_G^+ & & \\ C_{G1} & \underset{\beta'}{\overset{4\alpha'}{\rightleftarrows}} & C_{G2} & \underset{2\beta'}{\overset{3\alpha'}{\rightleftarrows}} & C_{G3} & & \end{array}$$

where $k_{G2}^- = 64k_G^-$ and $k_{G3}^- = (64)^2k_G^-$. For simplicity, the notations for the state of the system and the probability that the system is in that state are the same. The channel kinetic scheme can be written as differential equations using the law of mass action

$$\frac{dC_1}{dt} = \beta C_2 + k_G^- C_{G1} - (4\alpha + k_G^+)C_1 \quad (3)$$

$$\frac{dC_2}{dt} = 4\alpha C_1 + 2\beta C_3 + k_{G2}^- C_{G2} - (\beta + 3\alpha + k_G^+)C_2 \quad (4)$$

$$\frac{dC_3}{dt} = 3\alpha C_2 + 3\beta C_4 + k_{G3}^- C_{G3} - (2\beta + 2\alpha + k_G^+)C_3 \quad (5)$$

$$\frac{dC_4}{dt} = 2\alpha C_3 + 4\beta O - (3\beta + \alpha)C_4 \quad (6)$$

$$\frac{dC_{G1}}{dt} = \beta' C_{G2} + k_G^+ C_1 - (4\alpha' + k_G^-)C_{G1} \quad (7)$$

$$\frac{dC_{G2}}{dt} = 4\alpha' C_{G1} + 2\beta' C_{G3} + k_G^+ C_2 - (\beta' + 3\alpha' + k_{G2}^-)C_{G2} \quad (8)$$

$$\frac{dC_{G3}}{dt} = 3\alpha' C_{G2} + k_G^+ C_3 - (2\beta' + k_{G3}^-)C_{G3} \quad (9)$$

The probability that a channel is open is obtained from the conservation equation $O = 1 - C_1 - C_2 - C_3 - C_4 - C_{G1} - C_{G2} - C_{G3}$. The probability that a channel is in a reluctant state will be used later, $C_G = C_{G1} + C_{G2} + C_{G3}$. Voltage-dependent forward (α) and backward (β) rates are (in ms^{-1})

$$\alpha = 0.45e^{V/22} \quad \beta = 0.015e^{-V/14} \quad (10)$$

$$\alpha' = \alpha/8 \quad \beta' = 8\beta \quad (11)$$

The G protein binding rate (k_G^+, in ms^{-1}) is chosen to be a sigmoidal function of the fraction (a) of bound autoreceptors

$$k_G^+ = \frac{3a}{680 + 320a} \quad (12)$$

The unbinding rate, k_G^-, is set according to the G$\beta\gamma$ dimer simulated, as described later. Detailed descriptions of this channel model are given in Boland and Bean (1993) and Bertram and Behan (1999).

A very simple model is used for transmitter exocytosis, which assumes that Ca^{2+} must bind to a single site for exocytosis to occur. This model purposely omits synaptic enhancement due to the buildup of free or bound Ca^{2+} (Bertram et al. 1996; Zucker 1996) and depression due to the depletion of readily releasable vesicles (Abbott et al. 1997; Zucker 1989). These are omitted so that the effects of G protein inhibition and relief of inhibition can be studied independently of other modulatory mechanisms. The effects of relief of G protein inhibition on synaptic facilitation were addressed in a previous computational study (Bertram and Behan 1999), and a comparison of this form of depression with vesicle depletion was made in Bertram (2001). In the present model, transmitter release probability (R) is given by

$$\frac{dR}{dt} = k_r^+ Ca(1-R) - k_r^- R \quad (13)$$

where $k_r^+ = 0.15\ \mu\text{M}^{-1}\text{ms}^{-1}$, $k_r^- = 2.5\ \text{ms}^{-1}$, and Ca is the average domain Ca^{2+} concentration (in μM) at the mouth of an open Ca^{2+} channel, assumed to be colocalized with the transmitter release site. This depends on the probability that the channel is open (O), the Ca^{2+} concentration at an open channel (Ca_{open}) and a basal level of bulk Ca^{2+}, $Ca = OCa_{\text{open}} + 0.1$. The steady-state formula from Neher (1986) is used for Ca_{open}, assuming that no mobile Ca^{2+} buffers are present

$$Ca_{\text{open}} = \sigma/(2\pi D_c r) \quad (14)$$

where $D_c = 220\ \mu\text{m}^2\text{s}^{-1}$ is the Ca^{2+} diffusion coefficient (Allbritton et al. 1992), $r = 10$ nm is the assumed distance from the channel to the release site, and $\sigma = -5.182 \cdot i(V)$ is the Ca^{2+} flux through the channel. The single-channel current $i(V)$ is described by the Goldman-Hodgkin-Katz formula (Goldman 1943)

$$i(V) = \hat{g}_{Ca} P \frac{2FV}{RT}\left[\frac{Ca_{\text{ex}}}{1-\exp(2FV/RT)}\right] \quad (15)$$

with $\hat{g}_{Ca} = 1.2$ pS, $P = 6\ \text{mVmM}^{-1}$, $RT/F = 26.7$ mV, and $Ca_{\text{ex}} = 2$ mM. The $\hat{g}_{Ca} = 1.2$-pS single-channel conductance is used to approximate physiological Ca^{2+} concentrations. The domain Ca^{2+} equations and choice of parameters are discussed in detail in Bertram et al. (1999).

Transmitter concentration in the synaptic cleft is assumed to be proportional to the release probability, $T = \bar{T}R$, giving concentrations of several hundred micromolar during an action potential. For simulations of superthreshold postsynaptic responses $\bar{T} = 4$ mM, while $\bar{T} = 1$ mM for simulations of subthreshold responses. Transmitter in the cleft binds to presynaptic autoreceptors with binding and unbinding rates

determined from a cerebellar synapse (Dittman and Regehr 1997). The fraction of bound autoreceptors, used in *Eq. 12*, changes in time according to

$$\frac{da}{dt} = k_a^+ T(1 - a) - k_a^- a \quad (16)$$

where $k_a^+ = 0.2\ \text{mM}^{-1}\text{ms}^{-1}$ and $k_a^- = 0.0015\ \text{ms}^{-1}$.

Postsynaptic model

The model for postsynaptic membrane potential is similar to that for presynaptic membrane potential, with the addition of a synaptic current and the removal of the external applied current

$$C_m \frac{dV_{post}}{dt} = -(I_{Na,post} + I_{K,post} + I_{leak,post} + I_{syn}) \quad (17)$$

$$\frac{dn_{post}}{dt} = \alpha_n(1 - n_{post}) - \beta_n n_{post} \quad (18)$$

$$\frac{db}{dt} = k_b^+ T(1 - b) - k_b^- b \quad (19)$$

where α_n, β_n, and all currents depend on postsynaptic voltage. The synaptic current, $I_{syn} = g_{syn} b(V_{post} - V_{syn})$, depends also on the fraction of bound postsynaptic receptors, b, which changes in time according to *Eq. 19*, reflecting first-order binding of transmitter. The binding and unbinding rates are set to give a fast postsynaptic response, $k_b^+ = 2\ \text{mM}^{-1}\text{ms}^{-1}$, $k_b^- = 1\ \text{ms}^{-1}$. The synapse is assumed to be excitatory, with $V_{syn} = 0$ and $g_{syn} = 0.2\ \text{mScm}^{-2}$.

In the simulations shown in Figs. 3, 4, 8, and 9, there is one presynaptic neuron and one postsynaptic neuron. In network simulations, a 5×5 grid of "input layer" neurons projects to a 5×5 grid of "output layer" neurons. In the simulation shown in Fig. 5, *A* and *B*, each input layer cell projects to a single output layer cell; input cell (i, j) projects to output cell (i, j). In Figs. 5, *C* and *D*, 6, and 7 input cell (i, j) projects to output cells (i, j), $(i - 1, j)$, $(i + 1, j)$, $(i, j + 1)$, and $(i, j - 1)$. Input layer cells on the edge of the grid project to fewer cells, and output layer cells on the edge of the grid receive fewer synaptic inputs. For example, output edge cell (1, 2) receives input from input cells (1, 1), (1, 2), (1, 3), and (2, 2) only. Output corner cell (1, 1) receives input from input cells (1, 1), (1, 2), and (2, 1).

In simulations shown in Figs. 3, 4, 5, *A* and *B*, and 8, $\bar{T} = 4$ mM so that input from a single presynaptic cell can evoke a postsynaptic action potential (in the absence of G protein inhibition). In simulations shown in Figs. 5, *C* and *D*, 6 and 7, $\bar{T} = 1$ mM, and $k_b^+ = 1.1\ \text{mM}^{-1}\text{ms}^{-1}$, $k_b^- = 0.19\ \text{ms}^{-1}$ so that a single presynaptic cell is incapable of evoking a postsynaptic action potential. To maintain the same level of presynaptic autoreceptor activation, the binding rate is increased by a factor of four to $k_a^+ = 0.8\ \text{mM}^{-1}\text{ms}^{-1}$.

RESULTS

Kinetic slowing of N-type channels

With bath application of a G protein agonist, or transient expression of G$\beta\gamma$ dimers, a subpopulation of Ca^{2+} channels becomes bound by G$\beta\gamma$ and enters a reluctant state. Depolarization is thought to change the channel configuration, reflected in a rightward movement along the channel kinetic diagram, making it more likely that bound G$\beta\gamma$ dimers will unbind from reluctant channels. As a result, channels will move from a reluctant closed (RC) to a willing closed (WC) state. If the depolarization is sufficiently long, these channels can open (the willing open or WO state) and contribute to the macroscopic Ca^{2+} current. The extra steps involved in channel opening are the major reason for kinetic slowing. Another contributor to kinetic slowing is the slow opening of channels while in a reluctant state (reluctant openings, the RO state), which has been shown to occur during large depolarizations in N-type Ca^{2+} channels (Colecraft et al. 2000; Lee and Elmslie 2000). Since reluctant openings appear to be a minority of the delayed channel openings (Lee and Elmslie 2000), the RO state is not included in our mathematical model, and kinetic slowing is due entirely to the RC $\rightarrow$ WC $\rightarrow$ WO pathway.

Several studies have demonstrated that the degree of inhibition and kinetic slowing depends on the Gβ and Gγ isoforms comprising the activated G$\beta\gamma$ dimer (Arnot et al. 2000; Garcia et al. 1998; Ruiz-Velasco and Ikeda 2000; Zhou et al. 2000). To set kinetic parameters for the Ca^{2+} channel model, we focus here on data from Fig. 2 and from Arnot et al. (2000). Here, Gγ_2 and various Gβ subunits are co-transfected with N-type Ca^{2+} channels in HEK-tsa201 cells. A 100-ms test pulse to +20 mV is applied with or without a depolarizing prepulse to +150 mV (Fig. 2*A*). With the transfected G$\beta_1\gamma_2$ dimer, current recorded in the absence of a prepulse [$I(-\text{PP})$] was significantly reduced compared with that recorded following a prepulse [$I(+\text{PP})$] (Fig. 2*C*). The ratio $I(+\text{PP})$ to $I(-\text{PP})$ is a measure of the depolarization-induced relief of inhibition, or facilitation. The facilitation is smaller in the G$\beta_2\gamma_2$ transfected cells (Fig. 2*C*).

Facilitation decreases exponentially as the time interval between the prepulse and test pulse (Δt_1, Fig. 2) is increased (Fig. 1 in Arnot et al. 2000). It is at its greatest as $\Delta t_1 \rightarrow 0$. The exponential facilitation curve, extrapolated back to $\Delta t_1 = 0$, thus gives a measure of the real facilitation induced by the prepulse. This is shown in the *inset* to Fig. 2*B* for cells transfected with the G$\beta_1\gamma_2$ and G$\beta_2\gamma_2$ dimers. The greater real facilitation for G$\beta_1\gamma_2$-transfected cells suggests that G protein–coupled receptor activation of this subunit will have a greater modulatory impact on Ca^{2+} channels and downstream targets of Ca^{2+} influx. Real facilitation ratios for G$\beta_3\gamma_2$, G$\beta_4\gamma_2$, and G$\beta_5\gamma_2$ transfected cells are shown in Fig. 2 of Arnot et al. (2000), and demonstrate that real facilitation is greatest for G$\beta_1\gamma_2$ and G$\beta_3\gamma_2$ transfected cells, followed by G$\beta_2\gamma_2$ and G$\beta_4\gamma_2$. Cells transfected with G$\beta_5\gamma_2$ display no significant facilitation.

Kinetic slowing and prepulse facilitation are related in that both reflect the RC $\rightarrow$ WC transition, and thus depend on the G protein unbinding rate. Kinetic slowing in cells transfected with either G$\beta_1\gamma_2$ or G$\beta_2\gamma_2$ is illustrated in Fig. 2*C*. For a G$\beta_1\gamma_2$-transfected cell, channel activation is clearly much slower without a prepulse than with a prepulse. The *inset* shows exponential fits to the rising phase of the currents, providing a 2.90-ms time constant without prepulse and a 1.10-ms time constant with prepulse. For a G$\beta_2\gamma_2$-transfected cell there is less kinetic slowing, with activation time constants of 1.52 ms (−PP) and 1.15 ms (+PP). Kinetic slowing data are summarized in Fig. 2*B* for 22 cells transfected with G$\beta_1\gamma_2$ and 22 cells with G$\beta_2\gamma_2$. The larger extent of kinetic slowing exhibited by the G$\beta_1\gamma_2$ population is consistent with the greater prepulse facilitation induced by these dimers.

One important consequence of the large activation time constant −PP versus +PP is that there will be relatively few Ca^{2+} channel openings at the beginning of a train of action potentials, since each action potential is of very short duration. This is particularly true in the case of activation of G$\beta_1\gamma_2$

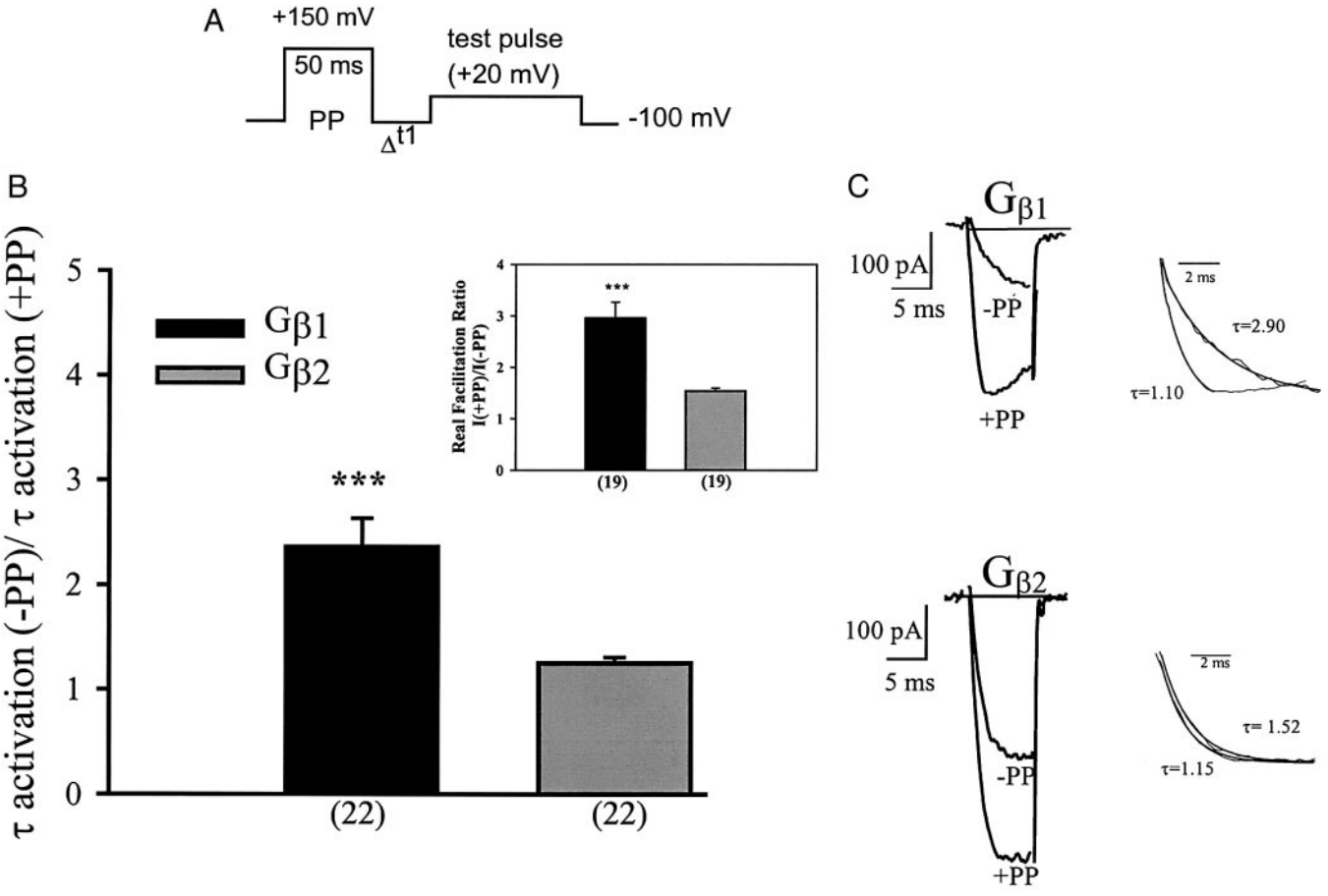

FIG. 2. Experimental data demonstrating kinetic slowing of an N-type channel. *A:* pulse protocol used to determine G protein real facilitation ratios after a strong depolarizing prepulse (PP) with $\Delta t1$ varied as described in METHODS. *B:* slowing of the Ca^{2+} channel mediated by $G\beta_1\gamma_2$ and $G\beta_2\gamma_2$. *Inset:* real facilitation ratios in the presence of $G\beta_1\gamma_2$ or $G\beta_2\gamma_2$. *C:* current traces illustrating kinetic slowing by $G\beta_1\gamma_2$ and $G\beta_2\gamma_2$. Current records were obtained in the absence of a PP or 2 ms following a 50-ms +150-mV PP. Current traces were recorded using a test pulse of +20 mV for 10 ms. *Inset:* a semiquantitative measure of the activation time constants using monoexponential fits of the activation time course. Error bars represent SE; numbers in parentheses reflect the number of experiments and asterisks denote significance ($P < 0.001$) relative to $G\beta_2\gamma_2$ values using Student's *t*-test.

dimers (Fig. 2*C*), where $I(-PP)$ is only about 15% of $I(+PP)$ 2 ms after the start of the test pulse. In fact, the prepulse-induced increase of the initial *slope* of the current is more important physiologically than the increase in the peak current, which may occur 10 ms or more after the start of the test pulse.

Calibration of the model was done by simulating the voltage-clamp protocol used in experiments (Fig. 2*A*). Since kinetic slowing is due largely to the delay in going from the RC to the WC state, it seems likely that the differential kinetic slowing exhibited by the $G\beta\gamma_2$ dimers is due largely to differences in the G protein unbinding rate, k_G^-. Indeed, we found that varying this parameter in the channel model was effective at producing a wide range of activation rates, with smaller values of k_G^- leading to more kinetic slowing. Using a fixed value of $k_G^+ = 0.035$ (ms^{-1}), the k_G^- were calibrated to produce activation time constant ratios similar to those for the $G\beta_1\gamma_2 - G\beta_4\gamma_2$ dimers (Fig. 3 of Arnot et al.). This is shown in Table 1. Simulations of the $G\beta_5\gamma_2$ dimer are not included since this appears to lead to little or no kinetic slowing. In this and subsequent simulations we assume identical G protein binding rates among the dimers, so that k_G^- is the sole parameter distinguishing one dimer from the next.

Frequency-dependent autoinhibition

The frequency dependence of autoinhibition is quite complex. On the one hand, more transmitter will be released at higher stimulus frequencies, yielding more G protein activation. On the other hand, the average presynaptic voltage is higher at higher stimulus frequencies, so there will be more relief of Ca^{2+} channel inhibition. Since Ca^{2+} channel inhibition in turn affects transmitter release probability, this means that both negative and positive feedback loops are present. The dominant feedback depends on the stimulus frequency, as we illustrate below.

A simulation with a single presynaptic and a single postsynaptic cell is shown in Fig. 3, where it is assumed that bound autoreceptors activate $G\beta_3\gamma_2$ dimers. Presynaptic action potentials are evoked (Fig. 3*A*) by a train of current pulses applied at 10 Hz for 1.5 s. Each action potential releases transmitter that

TABLE 1. *G protein unbinding and kinetic slowing in model*

	$G\beta_1\gamma_2$	$G\beta_2\gamma_2$	$G\beta_3\gamma_2$	$G\beta_4\gamma_2$
k_G^- (ms^{-1})	0.00025	0.01	0.0005	0.01
$\tau(-PP)/\tau(+PP)$	2.7	1.3	2.0	1.3

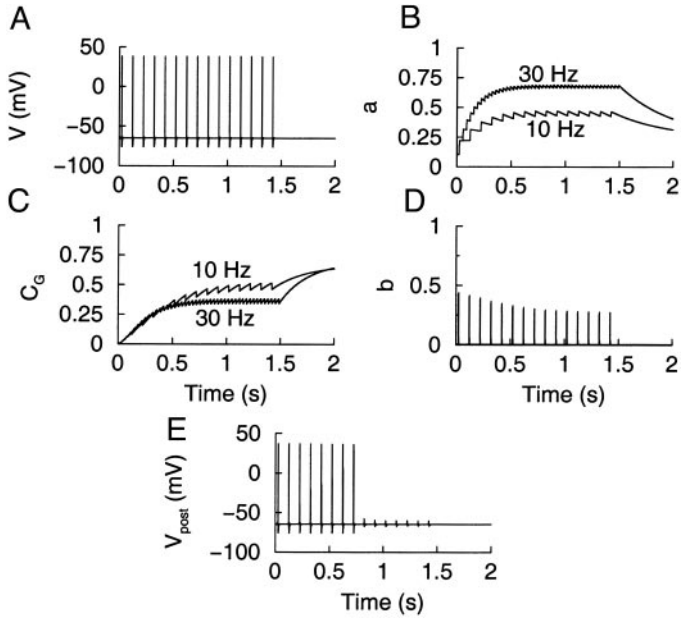

FIG. 3. Simulation with a single presynaptic and a single postsynaptic cell. *A:* a 10-Hz train of applied current pulses elicits presynaptic action potentials. *B:* during a 10-Hz or a 30-Hz train, the fraction of bound autoreceptors and the fraction of reluctant Ca^{2+} channels rise (*C*). *D:* the fraction of postsynaptic receptors bound with each evoked release of transmitter declines during the 10-Hz train, so that the postsynaptic voltage reaches spike threshold only during the 1st half of the train (*E*).

binds to postsynaptic receptors (Fig. 3*D*), depolarizing the postsynaptic cell to spike threshold during the first half of the pulse train (Fig. 3*E*). At the same time, transmitter molecules bind to presynaptic autoreceptors (Fig. 3*B*), activating G proteins and putting Ca^{2+} channels into a reluctant state (Fig. 3*C*). As the fraction of reluctant channels increases, the average domain Ca^{2+} concentration decreases, and so too does the transmitter release probability. Hence the fraction of postsynaptic receptors activated by presynaptic action potentials declines during the 10-Hz pulse train. Halfway through the train, excitatory postsynaptic currents (EPSCs) elicited by presynaptic action potentials are insufficient to reach the spike threshold, and postsynaptic action potentials are not produced. Hence the postsynaptic cell only responds transiently to the presynaptic impulse train; all later responses are filtered out by the G protein–mediated presynaptic inhibition. The inhibition of postsynaptic responses will remain throughout the duration of the pulse train, so a train of 30 presynaptic impulses will elicit the same postsynaptic response (8 postsynaptic impulses) as the train of 15 impulses.

At a higher stimulus frequency (e.g., 30 Hz) one might expect the postsynaptic response to be blunted to a greater extent than during the 10-Hz train, since the increase in transmitter release will result in more binding to presynaptic autoreceptors (Fig. 3*B*). However, the increased relief of inhibition that accompanies the increase in average presynaptic voltage will more than compensate for this, so that the fraction of reluctant channels will actually be lower than during the 10-Hz train (Fig. 3*C*). For this reason, the transmitter release is inhibited to a lesser extent during the 30-Hz train. The binding to postsynaptic receptors declines during the 30-Hz train (not shown) as it did during the 10-Hz train (Fig. 3*D*), but to a lesser extent, and the postsynaptic voltage reaches the spike threshold throughout the pulse train (not shown). Thus the lower-frequency signal is filtered out after a transient response, while the higher-frequency signal is transmitted in its entirety.

To determine the frequency range of input filtered out by autoinhibition, we performed simulations in which the presynaptic cell was stimulated for 10 s at frequencies ranging from 2 to 35 Hz. The number of postsynaptic action potentials generated by the resulting transmitter release was recorded. In the absence of presynaptic autoinhibition, the number of presynaptic and postsynaptic impulses is the same. However, with autoinhibition, the postsynaptic response can be blunted. Figure 4*A* shows the frequency response using the G protein unbinding rate calibrated for the $G\beta_1\gamma_2$ dimer. For frequencies $\geq$35 Hz the input impulse train is transmitted in its entirety to the postsynaptic cell. However, for frequencies $\leq$30 Hz the signal is filtered out; the postsynaptic cell generates only a short transient response. Thus the filter cut is between 30 and 35 Hz for the $G\beta_1\gamma_2$ dimer. Autoinhibition with the $G\beta_2\gamma_2$ dimer, which shows little kinetic slowing, allows signals of all frequencies $\geq$2 Hz to be transmitted (Fig. 4*B*), so the filter cut in this case is $<$2 Hz. Autoinhibition with the $G\beta_3\gamma_2$ dimer filters out input signals $\leq$15 Hz, while transmitting signals with frequencies $\geq$20 Hz, so the filter cut here is between 15 and 20 Hz. Finally, the unbinding kinetic rate determined for $G\beta_4\gamma_2$ is equal to that determined for $G\beta_2\gamma_2$, so the filtering properties are the same.

In summary, this computational study indicates that *1*) G protein–mediated autoinhibition can filter out low-frequency input (presynaptic) signals, thus acting as a high-pass filter, and *2*) the range of frequencies filtered out is different for different activated $G\beta\gamma$ dimers.

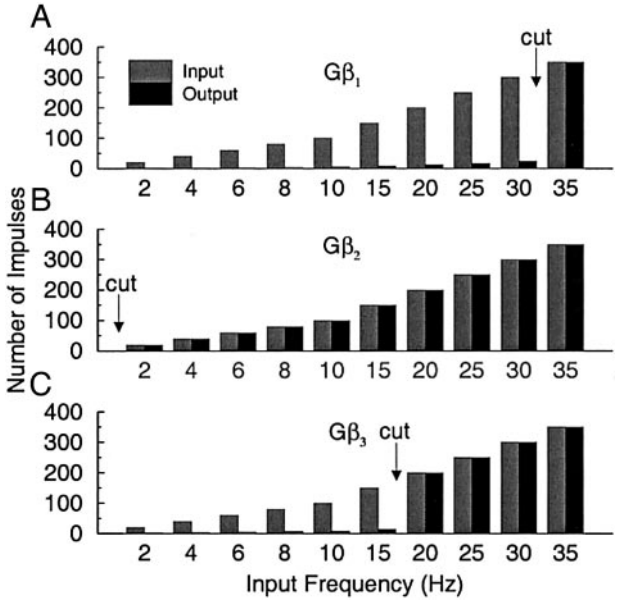

FIG. 4. Number of postsynaptic action potentials generated by presynaptic spike trains lasting 10 s, for a range of presynaptic stimulus frequencies. In the absence of autoinhibition, the number of postsynaptic spikes equals the number of presynaptic spikes (input, gray). Autoinhibition filters out the low-frequency spike trains, allowing high-frequency trains to pass in their entirety (output, black). The filter cut is different for different $G\beta\gamma$ dimers.

Autoinhibition increases spatial contrast

We now turn to some of the functional implications of the high-pass filtering mediated by autoinhibition. As a first example, we consider a 5 × 5 grid of presynaptic or input neurons projecting to a 5 × 5 grid of postsynaptic or output neurons, with each output neuron receiving input from exactly one input neuron (see METHODS). Each of the input neurons is subject to autoinhibition, acting via $G\beta_1\gamma_2$ dimers. The input neurons at locations (2, 2), (2, 4), (3, 3), (4, 2), and (4, 4) are stimulated at high frequencies, chosen randomly between 41 and 50 Hz, while other input cells are stimulated at low frequencies, chosen randomly between 1 and 10 Hz. The high-frequency input cells carry the "signal," while the low-frequency cells carry "noise." This is illustrated in Fig. 5*A*, where the number of impulses evoked during a 10-s stimulation is shown for each input cell using color and size coding (see figure caption). The large black squares correspond to the high-frequency signal, while the smaller colored squares correspond to noise at a range of frequencies (smaller squares for lower frequencies). Thus the spatially distributed signal, in the shape of an X, is degraded by surrounding noise.

A fundamental task of neural circuitry is to extract spatially distributed signals from the background noise. One way to do this is to employ lateral inhibition between input layer cells, so that neighboring cells inhibit one another (Shepherd 1998). High-frequency cells are more effective than low-frequency cells at inhibiting their neighbors, and as a consequence the low-frequency input is filtered out.

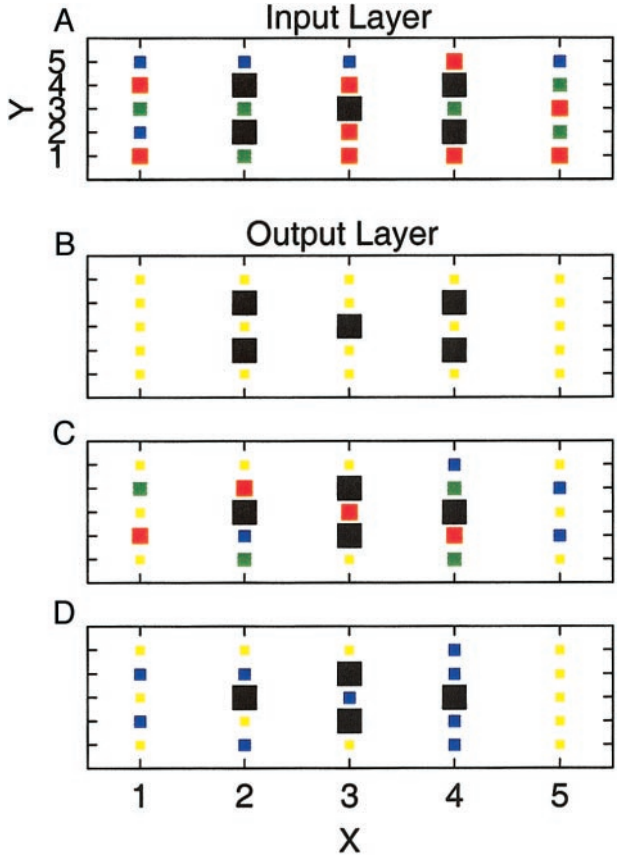

FIG. 5. *A:* 5 × 5 input layer of neurons stimulated at various frequencies and projecting directly onto a 5 × 5 output layer. *B:* each output cell receives a synaptic projection from 1 input cell. *C* and *D:* the input layer projects with nearest neighbor coupling to output layer cells. In *C* there is no presynaptic autoinhibition. Number of impulses in 10 s of stimulation (*N*) is color and size coded, with larger squares representing more impulses. Black, $N > 100$; red, $70 < N \leq 100$; green, $40 < N \leq 70$; blue, $10 < N < 40$; yellow, $N < 10$.

A second method for increasing spatial contrast is to employ G protein–mediated autoinhibition. As demonstrated in the previous section, autoinhibition preferentially filters out low-frequency input, while leaving high-frequency input intact. Thus the noise that was present in the input layer (Fig. 5*A*) is filtered out, and as a result the signal is much more prominent in the output layer (Fig. 5*B*). One advantage to this method of spatial contrast enhancement is that no circuitry is involved; each input neuron has feedback only onto itself. Another advantage is that the filter cut, and thus the definition of noise, is variable, depending on the $G\beta\gamma$ dimer activated by the autoreceptors (among other things). For example, while the $G\beta_1\gamma_2$ dimer used in Fig. 5 is effective at filtering the noise, the $G\beta_2\gamma_2$ dimer has no effect. Also, a 20-Hz signal would be considered noise by $G\beta_1\gamma_2$, and signal by $G\beta_3\gamma_2$. In the DISCUSSION we suggest possible mechanisms for time-dependent filter cuts.

As a second example, we again consider 5 × 5 grids of input and output neurons, but now each input cell projects to the corresponding output cell and its nearest neighbors. Several parameters have been adjusted so that release from a single presynaptic impulse is insufficient to bring a postsynaptic cell to the spike threshold (see METHODS). Instead, spike threshold is reached when two or more neighboring input cells fire at similar times, so that the postsynaptic EPSCs summate. Using the same input impulse distribution as in Fig. 5*A*, we now see a rather different output pattern even in the absence of autoinhibition (Fig. 5*C*). Output cells receiving input from two or more high-frequency "signal" input cells produce a high-frequency response, while others respond at low frequency. Thus the nearest-neighbor circuitry and the requirement for coincident inputs to evoke a response transform the spatial signal, and remove some of the noise (fewer red and green squares in Fig. 5*C* than in Fig. 5*A*). When $G\beta_1\gamma_2$ autoinhibition is included in the input layer cells, the output signal is as in Fig. 5*C*, but with reduced noise (Fig. 5*D*). Hence, even in this case where the circuitry performs a spatial transformation of the input signal, autoinhibition is effective at increasing the spatial contrast.

Autoinhibition increases fidelity of coincidence detection

For some tasks, the timing of synaptic input from several sources is crucial. This appears to be the case, for example, for sound localization and spatial orientation (Hopfield 1995). Associative learning is also thought to depend on action potential timing, in this case the coincident firing of associated pathways (Brown et al. 1990). One mechanism for coincidence detection is the requirement of temporal overlap of EPSCs to evoke a postsynaptic response. For perfect fidelity of coincidence detection, the output cell should fire only when input cells carrying high-frequency signals have coincident action potentials. Noise from low-frequency cells can reduce the fidelity by producing false positives. This occurs when an action potential in a low-frequency cell is coincident with an action potential in a high-frequency cell. We demonstrate here

that G protein–mediated autoinhibition can increase the fidelity of coincidence detection.

A scenario is considered in which 10 input cells project to a single output cell. As in Fig. 5, *C* and *D*, parameters are adjusted so that EPSCs must overlap to evoke a postsynaptic impulse. Two of the input cells carry high-frequency signals (80 and 100 Hz). The remaining input cells carry low-frequency noise, randomly chosen from 1 to 10 Hz. Autoinhibition is not included in the simulation. Figure 6 shows the voltage response of the single output cell (black) during a 100-ms simulation. Superimposed are excitatory postsynaptic potentials (EPSPs) evoked by transmitter released from the 80-Hz input cell alone and the 100-Hz input cell alone. Of the seven postsynaptic action potentials produced (truncated for clarity), only four are produced as the result of coincident input from the signal cells. These four "true positives," where the red and blue EPSPs overlap in such a way as to generate an impulse, are marked by arrows in the figure. The remaining three postsynaptic impulses, the false positives, are produced by the overlap of EPSCs from a signal cell and from a low-frequency noise cell. Thus the fidelity of coincidence detection of the high-frequency signals is low in this example.

High-pass filtering through autoinhibition can increase the fidelity of coincidence detection by reducing the noise. This is demonstrated in Fig. 7 for several combinations of signal frequencies. Here, simulations like the one above are carried out for 1 s of simulation time and the number of output spikes are counted, differentiating between true and false positives. For each simulation, eight of the input cells fire with frequencies between 1 and 10 Hz. The remaining two input cells fire at 40 and 60 Hz, 60 and 80 Hz, or 80 and 100 Hz. Figure 7*A* shows that, without autoinhibition, a large fraction of the postsynaptic impulses are false positives. When autoinhibition is introduced through activation of the $G\beta_1\gamma_2$ dimer, the number of false positives is greatly reduced (Fig. 7*B*). This is true for each combination of signal frequencies. The number of true positives is also reduced, since signal EPSCs that are only roughly coincident may not be sufficient to push the cell above the spike threshold without some coincident noise. However, the number of false positives is reduced to a much greater extent. As with spatial contrast enhancement, the increase in coincidence detection fidelity varies with the particular activated $G\beta\gamma$ dimer. The effect is maximized with the $G\beta_1\gamma_2$ dimer, and there is little or no effect with the $G\beta_2\gamma_2$ dimer.

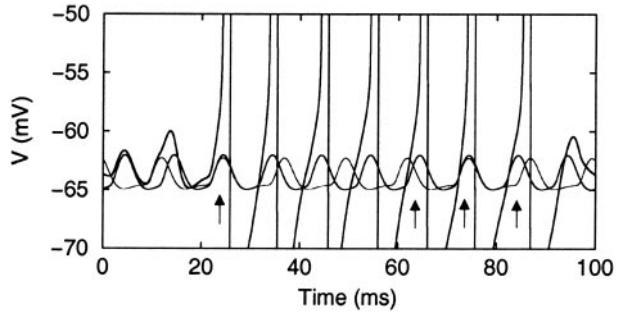

FIG. 6. Voltage response of a single output cell to subthreshold synaptic input from 10 input cells, with no autoinhibition. Two input cells fire at high frequencies, while the remaining 8 fire at low frequencies. Four impulses are generated by coincidence of high-frequency input (marked by arrows), 3 are generated by coincidence of low- and high-frequency input. Superimposed are excitatory postsynaptic potentials (EPSPs) from the 80-Hz and 100-Hz cells alone.

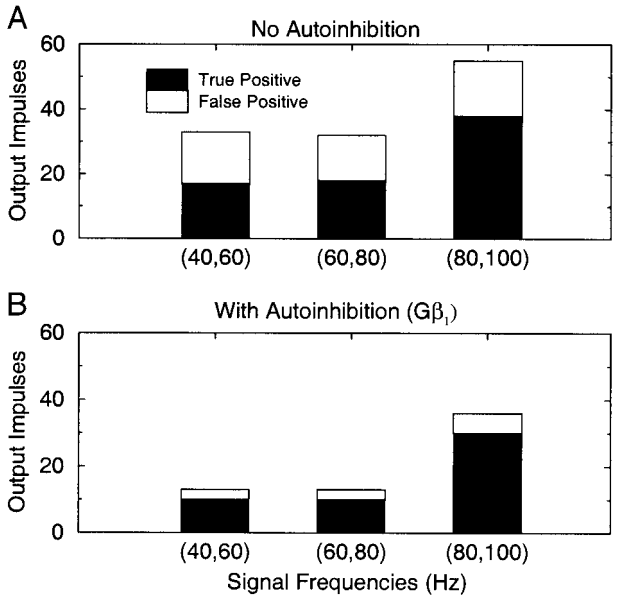

FIG. 7. True positives (■) and false positives (□) generated during a 1-s simulation, for 3 different combinations of signal frequencies. In each case, 8 of the 10 input cells fire at low frequencies between 1 and 10 Hz. *A:* with no autoinhibition there are many false positives. *B:* with $G\beta_1\gamma_2$ autoinhibition the fraction of false positives is greatly reduced, increasing the fidelity of coincidence detection.

Filter cut depends on autoreceptor kinetics

An important determinant of the high-pass filter cut is the dynamics of bound autoreceptor accumulation. The accumulation of bound autoreceptors during an impulse train depends on the impulse frequency, the proportionality constant ($\bar{T}$) between transmitter release probability and transmitter concentration in the synaptic cleft, and the autoreceptor binding (k_a^+) and unbinding (k_a^-) rates. In this section we examine how the filter cut is effected by changes in the autoreceptor unbinding rate.

We first consider the case in which autoreceptor binding leads to activation of $G\beta_3\gamma_2$ dimers. As in Fig. 4, a single input cell projects to a single output cell and parameters are adjusted so that a single uninhibited EPSC can evoke a postsynaptic action potential. Output spikes are counted during 10-s simulations, for a range of presynaptic spike frequencies. With the "control" autoreceptor unbinding rate, $k_a^- = 0.0015\ \text{ms}^{-1}$, the filter cut is between 15 and 20 Hz (Figs. 8*A* and 4*C*). When the unbinding rate is doubled, making the unbinding faster, the filter cut is lowered to between 6 and 8 Hz, allowing input at a lower frequency to pass through the filter (Fig. 8*B*). In this case there is less accumulation of bound autoreceptors, so that the depolarization-induced relief of inhibition dominates over a larger range of frequencies than in the control cell. When the unbinding rate is decreased by a factor of 10, making the unbinding much slower, the filter cut is shifted rightward, filtering out input at higher frequencies than in the control cell (Fig. 8*C*). Therefore the filter cut can be tuned up or down by the autoreceptor unbinding kinetics.

Tuning of the filter cut is explored more thoroughly by varying the autoreceptor unbinding rate by a factor λ, $k_a^- =$

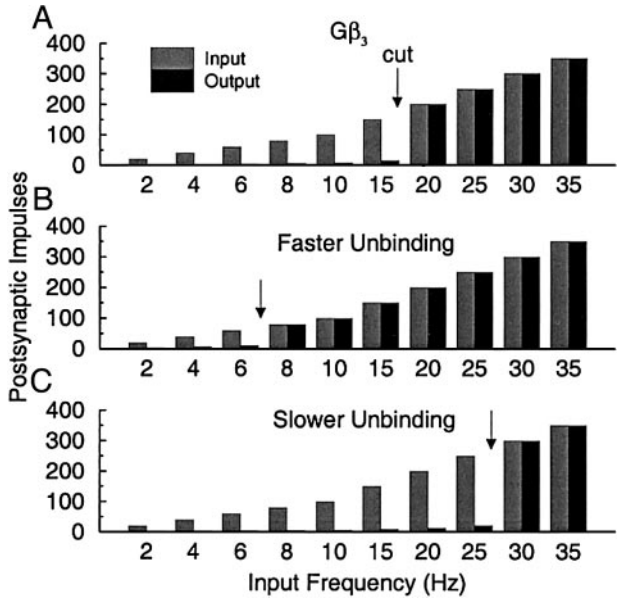

FIG. 8. The effect of changes in the autoreceptor unbinding rate (k_a^-) on autoinhibitory filtering with the $G\beta_3\gamma_2$ dimer. Presynaptic impulse trains of duration 10 s were simulated over a range of stimulus frequencies and the number of postsynaptic impulses counted. *A:* control, $k_a^- = 0.0015\ ms^{-1}$. *B:* faster unbinding, $k_a^- = 0.03\ ms^{-1}$, lowers the filter cut. *C:* slower unbinding, $k_a^- = 0.00015\ ms^{-1}$, raises the filter cut.

$\lambda k_{a,ctl}^-$, where $k_{a,ctl}^- = 0.0015\ ms^{-1}$ is the control unbinding rate. The stimulation protocol is as in Fig. 8, and for each $\lambda = 0.1, 0.25, 0.5, 1, 2, 4, 10$ the filter cut is determined. For presentation purposes, the cut is defined as the lowest frequency tested at which the input signal is transmitted in its entirety. For example, if a 15-Hz signal is filtered out and a 20-Hz signal is transmitted, then we define the cut to be 20 Hz. The lowest frequency tested is 2 Hz, so by default all cuts $\leq$2 Hz are defined as 2 Hz.

Figure 9 shows the filter cuts predicted by the model for three different $G\beta\gamma$ dimers over a range of values of λ (filter cuts for $G\beta_4\gamma_2$ are the same as for $G\beta_2\gamma_2$). With $\lambda = 10$ all input trains tested are passed in their entirety, regardless of the particular $G\beta\gamma$ dimer activated. For lower unbinding rates (smaller λ), the filter cut depends on the activated dimer. The filter cut for the $G\beta_2\gamma_2$ (and $G\beta_4\gamma_2$) dimer is always 2 Hz, regardless of the autoreceptor unbinding rate. This reflects the very weak kinetic slowing associated with this dimer (Fig. 2). The filter cuts for the $G\beta_1\gamma_2$ and $G\beta_3\gamma_2$ dimers are >2 Hz for most values of λ, indicating that some filtering is taking place. Indeed, the filter cut is as high as 45 Hz for $G\beta_1\gamma_2$ and 35 Hz for $G\beta_3\gamma_2$ when the autoreceptor unbinding rate is very low. This tunable filter cut would allow "low-frequency noise" to be defined in many different ways at different synapses, depending on the specific $G\beta\gamma$ dimer(s) activated and the unbinding kinetics of the G protein–coupled autoreceptor. Although we have shown the effects of tuning only one parameter, k_a^-, other parameters that could be tuned include k_a^+ and $\bar{T}$. The qualitative effects of these parameters are the opposite of k_a^-. For example, decreasing the autoreceptor binding rate k_a^+ shifts the filter cut to lower frequencies, just as does increasing the unbinding rate k_a^-. However, the magnitude of the change in the filter cut when k_a^+ is halved, for example, is not the same as when k_a^- is doubled. Thus it is not the autoreceptor dissociation constant alone that sets the filter cut, but the detailed kinetics of binding and unbinding.

DISCUSSION

Kinetic slowing is a prominent feature of G protein–mediated inhibition of Ca^{2+} channels, and the extent of slowing depends on the $G\beta\gamma$ dimer activated by the G protein–coupled receptor. Transfection of HEK cells with the $G\beta_1\gamma_2$ dimer produces significant slowing of co-transfected N-type Ca^{2+} channels, while transfection of $G\beta_2\gamma_2$ produces little slowing (Fig. 2). The $G\beta_3\gamma_2$ dimer also produces significant slowing, while $G\beta_4\gamma_2$ produces little and $G\beta_5\gamma_2$ is ineffective (Arnot et al. 2000). Given the short duration of action potentials, the most useful measure of the impact of slowing under physiological conditions is the decrease in the initial slope of the Ca^{2+} current during a test depolarization. Using short 10-ms test depolarizations, we have demonstrated that the initial slope of $G\beta_1\gamma_2$ is much reduced compared to the slope following a depolarizing prepulse (Fig. 2*C*), so that relatively few channels open during a single action potential or during the first few action potentials in a train. Williams et al. (1997) have demonstrated that trains of action potential–like depolarizations can relieve G protein inhibition of N-type channels, so that more channels will open during later impulses in the train. In contrast to $G\beta_1\gamma_2$, $G\beta_2\gamma_2$ has relatively little effect on the initial current slope (Fig. 2*C*), so this dimer will modulate the dynamics of Ca^{2+} entry to a lesser extent. We also note that the time constants for current activation in the presence of either $G\beta_1\gamma_2$ or $G\beta_2\gamma_2$ are relatively small compared with those observed in native cells in the presence of G protein agonists, particularly carbachol. The larger native time constant may reflect the net effect of many channel or G protein modulators, not included in our model.

Our primary goal was to predict, using computational modeling, the impact that kinetic slowing mediated by different $G\beta\gamma_2$ dimers would have on synaptic transmission if N-type channels, G proteins, and G protein autoreceptors were expressed in synaptic terminals. To this end, we calibrated a computational model of a G protein–regulated N-type Ca^{2+} channel to the G protein unbinding kinetics inferred from kinetic slowing data present here (Fig. 2) and in Arnot et al. (2000). With this, it was demonstrated that G protein–mediated autoinhibition acts as a high-pass filter, inhibiting the response

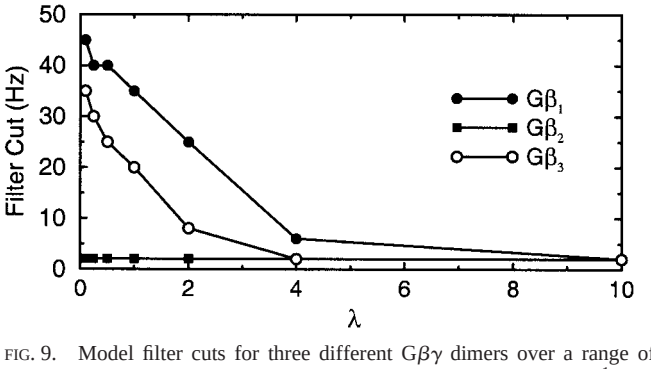

FIG. 9. Model filter cuts for three different $G\beta\gamma$ dimers over a range of autoreceptor unbinding rates ($k_a^- = \lambda k_{a,ctl}^-$), where $k_{a,ctl}^- = 0.0015\ ms^{-1}$. The filter cut varies over a large frequency range when $G\beta_1\gamma_2$ or $G\beta_3\gamma_2$ dimers are activated. There is little or no filtering when $G\beta_2\gamma_2$ or $G\beta_4\gamma_2$ dimers are activated.

to low-frequency impulse trains while transmitting high-frequency trains in their entirety (Fig. 3). This is consistent with experimental data from bullfrog sympathetic ganglia, showing prominent muscarinic autoinhibition during 1- to 5-Hz presynaptic impulse trains, but not during 20-Hz trains (Shen and Horn 1996). The high-pass filtering mediated by G protein–coupled autoreceptors is in sharp contrast to the low-pass filtering performed by vesicle depletion (Bertram 2001).

A key result of this study is that the filter cut, the input frequency below which signals are filtered, is different for the various $G\beta\gamma$ dimers, due to differences in kinetic slowing (Fig. 4). At present, there are 5 known $G\beta$ and 11 known $G\gamma$ isoforms (Betty et al. 1998; Morris and Malbon 1999), so there are potentially 55 different $G\beta\gamma$ dimers. The different $G\beta$ and $G\gamma$ isoforms are distributed widely throughout the rat brain (Betty et al. 1998), although their distribution in synaptic terminals is not currently known. The wide range of filter cuts predicted in this study suggests that autoreceptor filtering may provide exquisite control over which inputs represent "signal" and are transmitted, and which represent "noise" and are filtered out. Further enhancing the range of variability is recent data showing that the efficacy of G protein agonists (Canti et al. 2000) and, more specifically, $G\beta\gamma$ dimers (Feng et al. 2001) depends on which of the four Ca^{2+} channel β subunit isoforms is expressed in the cell. For example, the $G\beta_5\gamma_2$ isoform induced little if any inhibition of N-type channels containing the β_{1b} subunit, while inhibition of channels containing the β_{2a} subunit was significant (Arnot et al. 2000; Feng et al. 2001).

Using a network of input and output neurons, we found that the spatial contrast between a spatially distributed high-frequency signal and low-frequency noise can be dramatically improved by autoinhibition (Fig. 5). This could be a very useful mechanism for cleaning up noisy sensory input, and it has the advantage that no input-layer circuitry is needed, as is the case for spatial contrast enhancement through lateral inhibition (Shepherd 1998). Another advantage is that the filter cut, and thus the definition of noise, can be adjusted to different values at different synapses, according to the types of $G\beta\gamma$ dimers activated.

Another finding of this study is that autoinhibition can improve the fidelity of coincidence detection by reducing noise (Figs. 6 and 7). That is, if the function of the postsynaptic cell is to fire only when high-frequency signals are coincident, autoinhibition decreases the number of "false positives," where a postsynaptic response is evoked by coincidence of a high-frequency signal with low-frequency noise. Again, this is accomplished without input-layer circuitry, and the definition of noise is determined by the $G\beta\gamma$ dimer or mix of $G\beta\gamma$ dimers activated by the presynaptic autoreceptors.

In our computational model we have made the assumption that $G\beta\gamma_2$ dimers differ only in the G protein unbinding rate. Although calibration of this parameter is effective in reproducing the kinetic slowing reported here and in Arnot et al. (2000), it is likely that the dimers differ in several biophysical parameters. In our analysis of high-pass filtering, we demonstrated how differences in kinetic slowing exhibited by the dimers translates into differences in the filter cut. However, it is important to realize that there are many potential biophysical processes that help determine the filter cuts. These include, but are not limited to, the binding/unbinding rates of transmitter to the autoreceptor, the binding/unbinding rates of G proteins to the Ca^{2+} channel, and the distribution of inhibited and uninhibited channels in the synaptic terminal. Synapse-to-synapse differences in these parameters can potentially lead to a wider range of filter cuts than is shown in Fig. 4. The effect of variation of the rate of transmitter unbinding from autoreceptors was explored in Figs. 8 and 9. Faster unbinding yields less accumulation of activated G proteins, so the impulse frequency required to overcome channel inhibition is lower, shifting the filter cut to a lower frequency. Slower transmitter unbinding has the opposite effect. For the $G\beta_1\gamma_2$ and $G\beta_3\gamma_2$ dimers, variation in the transmitter unbinding rate can shift the filter cut over a wide range of frequencies, while the unbinding rate of $G\beta_2\gamma_2$ and $G\beta_4\gamma_2$ is too rapid to produce significant filtering regardless of the transmitter unbinding rate (Fig. 9).

One intriguing feature of G protein inhibition of Ca^{2+} channels is the multiplicity of regulatory genetic and chemical pathways. Both G protein activation and the rate of hydrolysis of activated G protein α subunits (which can terminate G protein inhibition via binding of GDP-bound α subunits to $G\beta\gamma$ dimers) can be controlled by regulators of G protein signaling (RGS proteins), which accelerate GTPase activity (Chen and Lambert 2000; Hepler 1999; Kammermeier and Ikeda 1999; Zhou et al. 2000). N-type channels are also regulated by protein kinase C, which has the dual effect of upregulating channel activity and antagonizing G protein inhibition (Hamid et al. 1999; Swartz 1993; Swartz et al. 1993; Zamponi et al. 1997). G protein inhibition of N-type Ca^{2+} channels is also modulated by the synaptic SNARE protein syntaxin 1A. Channels bound to syntaxin 1A are more readily inhibited by G proteins, raising the possibility that syntaxin 1A physically colocalizes $G\beta\gamma$ with N-type channels (Jarvis et al. 2000; Stanley and Mirotznik 1997). An interesting genetic feedback mechanism is suggested by a recent study showing that Ca^{2+} entry through P/Q-type channels induces expression of syntaxin 1A, thus increasing the effectiveness of G protein inhibition of N-type channels (Sutton et al. 1999). These and possibly other modulatory pathways provide the means for *dynamic regulation* of G protein–mediated synaptic filtering. That is, the filter cut may not only vary from synapse to synapse, but it may also vary with time in an individual synapse.

Several simplifying assumptions were made in our presynaptic and postsynaptic mathematical models, in addition to those described above. It was assumed that N-type channels were the only Ca^{2+} channel type present in the terminal, and that each presynaptic vesicle is colocalized with a single Ca^{2+} channel, with exocytosis occurring upon binding of a single Ca^{2+} ion. Each of these channels was assumed to be subject to G protein inhibition. A previous computational study showed that this may overestimate the relief of Ca^{2+} current during trains of action potentials. A more likely scenario is that one subpopulation of Ca^{2+} channels is not subject to G protein inhibition, so that the relief of inhibition during an impulse train is reduced (Bertram and Behan 1999). It was assumed that there is no facilitation of transmitter release due to the buildup of free or bound Ca^{2+} ions, and that there is no depletion of readily releasable vesicles. It was assumed that transmitter concentration in the cleft is proportional to the transmitter release probability, and that postsynaptic receptors do not desensitize. The postsynaptic cell was modeled as a single compartment, neglecting the effects of current flow between

neighboring dendritic spines. Finally, it was assumed that all G protein–mediated channel inhibition can be relieved by depolarization. In fact, there is evidence for a voltage-independent form of inhibition (Hille 1992; Luebke and Dunlap 1994), and in synapses exhibiting both voltage-dependent and voltage-independent forms the relief from inhibition induced by trains of action potentials would be less than what is predicted by our model. Relaxing all of these assumptions would make the model, and its interpretation, unwieldy. However, relaxation of subsets of the assumptions is possible and may reveal additional phenomena to those discussed here.

In summary, this study demonstrates that autoinhibition mediated by G protein–coupled receptors can act as a high-pass filter, and that the filter properties are determined by the specific G$\beta\gamma$ isoform activated by the receptors. We show that high-pass filtering can enhance spatial contrast and can improve the fidelity of coincidence detection. The dependence of the filter cut on several biophysical parameters allows for variations in filter properties from synapse to synapse, and has the potential for dynamic regulation through genetic and biochemical pathways.

G. W. Zamponi holds faculty scholarships from the Canadian Institutes of Health Research (CIHR), the Alberta Heritage Foundation for Medical Research, and the EJLB Foundation and holds the Novartis Chair for Schizophrenia Research. M. I. Arnot is the recipient of a postdoctoral fellowship from the Heart and Stroke Foundation of Canada. This work was also supported by a grant from the CIHR. R. Bertram was supported by National Science Foundation Grants DBI 9602233 and DMS 9981822.

REFERENCES

ABBOTT LF, VARELA JA, SEN K, AND NELSON SB. Synaptic depression and cortical gain control. *Science* 275: 220–224, 1997.

ALLBRITTON NL, MEYER T, AND STRYER L. Range of messenger action of calcium ion and inositol 1,4,5-trisphophate. *Science* 258: 1812–1815, 1992.

ARNOT MI, STOTZ SC, JARVIS SE, AND ZAMPONI GW. Differential modulation of N-type α_{1B} and P/Q-type α_{1A} calcium channels by different G protein β subunit isoforms. *J Physiol (Lond)* 527: 203–212, 2000.

BEAN BP. Neurotransmitter inhibition of neuronal calcium currents by changes in channel voltage dependence. *Nature* 340: 153–156, 1989.

BERTRAM R. Differential filtering of two presynaptic depression mechanisms. *Neural Comput* 13: 69–85, 2001.

BERTRAM R AND BEHAN M. Implications of G-protein–mediated Ca^{2+} channel inhibition for neurotransmitter release and facilitation. *J Comput Neurosci* 7: 197–211, 1999.

BERTRAM R, SHERMAN A, AND STANLEY EF. Single-domain/bound calcium hypothesis of transmitter release and facilitation. *J Neurophysiol* 75: 1919–1931, 1996.

BERTRAM R, SMITH GD, AND SHERMAN A. A modeling study of the effects of overlapping Ca^{2+} microdomains on neurotransmitter release. *Biophys J* 76: 735–750, 1999.

BETTY M, HARNISH SW, RHODES KJ, AND COCKETT MI. Distribution of heterotrimeric G-protein β and γ subunits in the rat brain. *Neuroscience* 85: 475–486, 1998.

BITO H, DEISSEROTH K, AND TSIEN RW. Ca^{2+}-dependent regulation in neuronal gene expression. *Curr Opin Neurobiol* 7: 419–429, 1997.

BOEHM S AND BETZ H. Somatostatin inhibits excitatory transmission at rat hippocampal synapses via presynaptic receptors. *J Neurosci* 17: 4066–4075, 1997.

BOLAND LM AND BEAN BP. Modulation of N-type calcium channels in bullfrog sympathetic neurons by luteinizing hormone-releasing hormone: kinetics and voltage dependence. *J Neurosci* 13: 516–533, 1993.

BRODY DL, PATIL PG, MULLE JG, SNUTCH TP, AND YUE DT. Bursts of action potential waveforms relieve G-protein inhibition of recombinant P/Q-type Ca^{2+} channels in HEK 293 cells. *J Physiol (Lond)* 769: 637–644, 1997.

BRODY DL AND YUE DT. Relief of G-protein inhibition of calcium channels and short-term synaptic facilitation in cultured hippocampal neurons. *J Neurosci* 20: 889–898, 2000.

BROWN TH, KAIRISS EW, AND KEENAN CL. Hebbian synapses: biophysical mechanisms and algorithms. *Annu Rev Neurosci* 13: 475–511, 1990.

CANTI C, BOGDANOV Y, AND DOLPHIN AC. Interaction between G proteins and accessory β subunits in the regulation of α1B calcium channels in xenopus oocytes. *J Physiol (Lond)* 527: 419–432, 2000.

CHEN G AND VAN DEN POL AN. Adenosine modulation of calcium currents and presynaptic inhibition of GABA release in suprachiasmatic and arcuate nucleus neurons. *J Neurophysiol* 77: 3035–3047, 1997.

CHEN G AND VAN DEN POL AN. Presynaptic $GABA_B$ autoreceptor modulation of P/Q-type calcium channels and GABA release in rat suptrachiasmatic nucleus neurons. *J Neurosci* 18: 1913–1922, 1998.

CHEN H AND LAMBERT NA. Endogenous regulators of G protein signaling proteins regulate presynaptic inhibition at rat hippocampal synapses. *Proc Natl Acad Sci USA* 97: 12810–12815, 2000.

COLECRAFT HM, PATIL PG, AND YUE DT. Differential occurrence of reluctant openings in G-protein-inhibited N- and P/Q-type calcium channels. *J Gen Physiol* 115: 175–192, 2000.

DITTMAN JS AND REGEHR WG. Contributions of calcium-dependent and calcium-independent mechanisms to presynaptic inhibition at a cerebellar synapse. *J Neurosci* 16: 1623–1633, 1996.

DITTMAN JS AND REGEHR WG. Mechanism and kinetics of heterosynaptic depression at a cerebellar synapse. *J Neurosci* 17: 9048–9059, 1997.

DIVERSÉ-PIERLUISSI M, MCINTIRE WE, MYUNG C-S, LINDORFER MA, GARRISON JC, GOY MF, AND DUNLAP K. Selective coupling of G protein $\beta\gamma$ complexes to inhibition of Ca^{2+} channels. *J Biol Chem* 275: 28380–28385, 2000.

DUNWIDDIE TV AND HAAS HL. Adenosine increases synaptic facilitation in the in vitro rat hippocampus: evidence for a presynaptic site of action. *J Physiol (Lond)* 369: 365–377, 1985.

FENG Z-P, ARNOT MI, DOERING CJ, AND ZAMPONI GW. Calcium channel β subunits differentially regulate the inhibition of N-type channels by individual Gβ isoforms. *J Biol Chem.* 276: 45051–45058, 2001.

GARCIA DE, LI B, GARCIA-FERREIRO RE, HERNANDEZ-OCHOA EO, YAN K, GAUTAM N, CATTERALL WA, MACKIE K, AND HILLE B. G-protein β-subunit specificity in the fast membrane-delimited inhibition of Ca^{2+} channels. *J Neurosci* 18: 9163–9170, 1998.

GOLDMAN DE. Potential, impedance, and rectifications in membranes. *J Gen Physiol* 27: 36–60, 1943.

HAMID J, NELSON D, SPAETGENS R, DUBEL SJ, SNUTCH TP, AND ZAMPONI GW. Identification of an integration center for the cross-talk between protein kinase C and G protein modulation of N-type calcium channels. *J Biol Chem* 274: 6195–6202, 1999.

HEPLER JR. Emerging roles for RGS proteins in cell signaling. *Trends Pharmacol Sci* 20: 376–382, 1999.

HERLITZE S, GARCIA DE, MACKIE K, HILLE B, SCHEUER T, AND CATTERALL WA. Modulation of Ca^{2+} channels by G-protein $\beta\gamma$ subunits. *Nature* 380: 255–262, 1996.

HILLE B. G-protein–coupled mechanisms and nervous signaling. *Neuron* 9: 187–195, 1992.

HODGKIN AL AND HUXLEY AF. A quantitative description of membrane current and its application to conduction and excitation in nerve. *J Physiol (Lond)* 117: 500–544, 1952.

HOPFIELD JJ. Pattern recognition computation using action potential timing for stimulus representation. *Nature* 376: 33–36, 1995.

IKEDA SR. Voltage-dependent modulation of N-type calcium channels by G-protein $\beta\gamma$ subunits. *Nature* 380: 255–262, 1996.

ISAACSON JS, SOLIS JM, AND NICOLL RA. Local and diffuse synaptic actions of GABA in the hippocampus. *Neuron* 10: 165–175, 1993.

JARVIS SE, MAGGA JM, BEEDLE AM, BRAUN JEA, AND ZAMPONI GW. G protein modulation of N-type calcium channels is facilitated by physical interactions between syntaxin 1A and G$\beta\gamma$. *J Biol Chem* 275: 6388–6394, 2000.

KAJIKAWA Y, SAITOH N, AND TAKAHASHI T. GTP-binding protein $\beta\gamma$ subunits mediate presynaptic calcium current inhibition by $GABA_B$ receptor. *Proc Natl Acad Sci USA* 98: 8054–8058, 2001.

KAMMERMEIER PJ AND IKEDA SR. Expression of RGS2 alters the coupling of metabotropic glutamate receptor 1a to M-type K^+ and N-type Ca^{2+} channels. *Neuron* 22: 819–829, 1999.

LEE HK AND ELMSLIE KS. Reluctant gating of single N-type calcium channels during neurotransmitter-induced inhibition in bullfrog sympathetic neurons. *J Neurosci* 20: 3115–3128, 2000.

LLINÁS R, SUGIMORI M, AND SILVER RB. Microdomains of high calcium concentration in a presynaptic terminal. *Science* 256: 677–679, 1992.

LUEBKE JI AND DUNLAP K. Sensory neuron N-type calcium currents are inhibited by both voltage-dependent and -independent mechanisms. *Pflügers Arch* 428: 499–507, 1994.

MORRIS AJ AND MALBON CC. Physiological regulation of G-protein linked signalling. *Physiol Rev* 79: 1373–1430, 1999.

NEHER E. Concentration profiles of intracellular calcium in the presence of a diffusible chelator. In: *Calcium Electrogenesis and Neuronal Functioning*, edited by Heinemann U, Klee M, Neher E, and Singer W. Berlin: Springer-Verlag, 1986, p. 80–96.

PATIL PG, DE LEON M, REED RR, DUBEL S, SNUTCH TP, AND YUE DT. Elementary events underlying voltage-dependent G-protein inhibition of N-type calcium channels. *Biophys J* 71: 2509–2521, 1996.

QIAN J, COLMERS WF, AND SAGGAU P. Inhibition of synaptic transmission by neuropeptide Y in rat hippocampal area CA1: modulation of presynaptic Ca^{2+} entry. *J Neurosci* 17: 8169–8177, 1997.

RINZEL J AND ERMENTROUT GB. Analysis of neural excitability and oscillations. In: *Methods in Neuronal Modeling: From Synapses to Networks*, edited by Koch C and Segev I. Cambridge, MA: MIT Press, 1989, p. 135–169.

RUIZ-VELASCO V AND IKEDA SR. Multiple G-protein $\beta\gamma$ combinations produce voltage-dependent inhibition of N-type calcium channels in rat superior cervical ganglion neurons. *J Neurosci* 20: 2183–2191, 2000.

SABATINI BL AND REGEHR WG. Control of neurotransmitter release by presynaptic waveform at the granule cell to Purkinje cell synapse. *J Neurosci* 17: 3425–3435, 1997.

SHEN K-Z AND JOHNSON SW. Presynaptic $GABA_B$ and adenosine A_1 receptors regulate synaptic transmission to rat substantia nigra reticulata neurones. *J Physiol (Lond)* 505: 153–163, 1997.

SHEN W-X AND HORN JP. Presynaptic muscarinic inhibition in bullfrog sympathetic ganglia. *J Physiol (Lond)* 491: 413–421, 1996.

SHEPHERD GM. *The Synaptic Organization of the Brain.* New York: Oxford University Press, 1998, p. 30–32.

SIMON S AND LLINÁS R. Compartmentalization of the submembrane calcium activity during calcium influx and its significance in transmitter release. *Biophys J* 48: 485–498, 1985.

STANLEY EF AND MIROTZNIK RR. Cleavage of syntaxin prevents G-protein regulation of presynaptic calcium channels. *Nature* 385: 340–343, 1997.

SUTTON KG, MCRORY JE, GUTHRIE H, MURPHY TH, AND SNUTCH TP. P/Q-type calcium channels mediate the activity-dependent feedback of syntaxin-1A. *Nature* 401: 800–804, 1999.

SWARTZ KJ. Modulation of Ca^{2+} channels by protein kinase C in rat central and peripheral neurons: disruption of G protein–mediated inhibition. *Neuron* 11: 305–320, 1993.

SWARTZ KJ, MERRIT A, BEAN BP, AND LOVINGER DM. Protein kinase C modulates glutamate receptor inhibition of Ca^{2+} channels and synaptic transmission. *Nature* 361: 165–168, 1993.

TAKAHASHI T, KAJIKAWA Y, AND TSUJIMOTO R. G-protein–coupled modulation of presynaptic calcium currents and transmitter release by a $GABA_B$ receptor. *J Neurosci* 18: 3138–3146, 1998.

TSIEN RW AND TSIEN RY. Calcium channels, stores, and oscillations. *Annu Rev Cell Biol* 6: 715–760, 1990.

WILLIAMS S, SERAFIN M, MÜHLETHALER M, AND BERNHEIM L. Facilitation of N-type calcium current is dependent on the frequency of action potential–like depolarizations in dissociated cholinergic basal forebrain neurons of the guinea pig. *J Neurosci* 17: 1625–1632, 1997.

WU L-G AND SAGGAU P. Adenosine inhibits evoked synaptic transmission primarily by reducing presynaptic calcium influx in area CA1 of hippocampus. *Neuron* 12: 1139–1148, 1994.

WU L-G AND SAGGAU P. Presynaptic inhibition of elicited neurotransmitter release. *Trends Neurosci* 20: 204–212, 1997.

ZAMPONI GW, BOURINET E, NELSON D, NARGEOT J, AND SNUTCH TP. Crosstalk between G proteins and protein kinase C mediate by the calcium channel α_1 subunit. *Nature* 385: 442–446, 1997.

ZAMPONI GW AND SNUTCH TP. Decay of prepulse facilitation of N type calcium channels during G protein inhibition is consistent with binding of a single $G_{\beta\gamma}$ subunit. *Proc Natl Acad Sci USA* 95: 4035–4039, 1998.

ZHANG J, ELLINOR PT, ALDRICH RW, AND TSIEN RW. Multiple structural elements in voltage-dependent Ca^{2+} channels support their inhibition by G proteins. *Neuron* 17: 991–1003, 1996.

ZHOU JY, SIDEROVSKI DP, AND MILLER RJ. Selective regulation of N-type Ca channels by different combinations of G-protein β/γ subunits and RGS proteins. *J Neurosci* 20: 7143–7148, 2000.

ZUCKER RS. Short-term synaptic plasticity. *Annu Rev Neurosci* 12: 13–31, 1989.

ZUCKER RS. Exocytosis: a molecular and physiological perspective. *Neuron* 17: 1049–1055, 1996.